ELSEVIER

International Journal of Heat and Fluid Flow 21 (2000) 480–488

International Journal of HEAT AND FLUID FLOW

www.elsevier.com/locate/ijhff

Near-wall turbulence structures in three-dimensional boundary layers

Anh-Tuan Le *, Gary N. Coleman [1], John Kim

Department of Mechanical and Aerospace Engineering, UCLA, Los Angeles, CA 90095-1597, USA

Abstract

We examine the structure of near-wall turbulence in three-dimensional boundary layers (3DBLs), which we approximate by applying an impulsive spanwise motion to the lower wall of a turbulent channel flow. Direct numerical simulation (DNS) data are analysed using probability density functions (PDFs), conditional-averaged quadrant analysis about Reynolds-stress-producing events, and visualization of vortices with the λ_2-criterion. The evidence suggests that mean three-dimensionality breaks up the symmetry and alignment of near-wall structures, disrupting their self-sustaining mechanisms, and thereby causing a reduction in the turbulence kinetic energy (TKE). © 2000 Begell House Inc. Published by Elsevier Science Inc. All rights reserved.

1. Introduction

In a three-dimensional boundary layer (3DBL) the mean flow direction changes with distance from the wall, and the turbulent stresses are not aligned with the mean shear. In many cases, the result is a decrease in TKE and Reynolds shear stress compared to an equivalent two-dimensional boundary layer (2DBL). Although 3DBLs exist in which these statistics increase (see listing in Johnston and Flack, 1996), the flowfields in those cases also contain adverse pressure gradients (not a 3D effect), which are known to increase the TKE in the outer regions of the boundary layer. In practice (for example, for the flow over a swept wing) the adverse pressure gradient can dominate over the 3D effects (Coleman et al., 1997). Even in such flows, however, three-dimensionality serves to damp the turbulence in the near-wall region. Moreover, the ratio of the turbulent shear stress to the TKE is generally found to decrease relative to 2DBLs, signifying a reduction in the effectiveness of the turbulence in extracting kinetic energy from the mean flow.

The mechanism by which the turbulence quantities discussed above are altered has been a subject of much debate. For example, Anderson and Eaton (1989) suggested that the spanwise flow reduces the strength of quasi-streamwise vortices having the opposite sign of streamwise vorticity to the mean spanwise flow, reducing the mixing that occurs between vortices of opposite signs. Shizawa and Eaton (1990) found that artificially-generated vortices of either sign embedded into the boundary layer decay faster than they would in a 2DBL, but vortices whose near-wall spanwise velocity is in the same direction as the crossflow produce weakened ejections. Littel and Eaton (1994) found that the crossflow inhibits strong *sweeps* from vortices having near-wall spanwise velocity in the same direction as the crossflow, while it inhibits strong *ejections* from vortices having spanwise velocity in the opposite direction. Kang et al. (1998) concluded that the asymmetries in the conditional averages of Littel and Eaton (1994) are only caused by non-Reynolds–stress-producing events. Sendstad and Moin (1992) advanced four mechanisms by which the spanwise crossflow affects particle trajectories in the vortical structures, each important at different times, which serve to generate lower Reynolds stress and break up the near-wall streaks. Their findings are, in general, consistent with those of Littel and Eaton. However, the mechanisms described by Sendstad and Moin assume that near-wall vortices are aligned horizontally in the 2D flow, act as independent units on the surrounding fluid, and respond in a 2D manner to the spanwise shear. More recent studies of coherent structures in 2DBLs, both experimental and numerical, indicate that near-wall turbulence structures generally have a finite inclination to the wall, and interact in a cooperative manner to perpetuate turbulence (e.g., Jeong et al., 1997; Tomkins et al., 1998).

In earlier work (Coleman et al., 1996) we found that applying mean spanwise shear $\partial W/\partial y$ anywhere in the near-wall region of an initially 2D flow reduces the mean streamwise skin friction, with the greatest reduction occurring when $\partial W/\partial y$ is applied between approximately $y^+ = 5$ and 15 (where y^+ is the wall-normal distance in wall units). While this finding has significant practical implications (indicating, for example, where drag-reduction control schemes should focus), it does not give a detailed picture of the manner in which mean three-dimensionality modifies near-wall structures in practice. The objective of the present study is to obtain additional insight into the behavior of the near-wall structures that are responsible for the observed changes in 3DBL turbulence, by employing a combination of statistical and visualization techniques. The results may lead to improvements in turbulence models and suggest new methods for turbulence control.

* Corresponding author. Fax: +1-310-206-4830.
E-mail address: anhtuan@seas.ucla.edu (A.-T. Le).
[1] Present address: School of Engineering Sciences, University of Southampton, Highfield, Southampton SO17 1BJ, UK.

0142-727X/00/$ - see front matter
PII: S0142-727X(00)00035-7

2. Approach

All solutions are obtained using DNS. Probability density functions (PDFs) of velocity and vorticity are used to analyse the data. We also employ the conditional-averaged quadrant analysis introduced by Kang et al. (1998). Vortical structures within the flowfields are visualized using the λ_2-criterion of Jeong and Hussain (1995), whereby vortices are associated with negative values of λ_2, defined as the second largest eigenvalue of the tensor $S_{ik}S_{kj} + \Omega_{ik}\Omega_{kj}$, where $S_{ij} = (u_{i,j} + u_{j,i})/2$ and $\Omega_{ij} = (u_{i,j} - u_{j,i})/2$ are the strain and rotation tensors, respectively. Here the subscripts (i, j, k) may have values $(1, 2, 3)$ which correspond respectively to the streamwise, wall-normal, and spanwise directions, such that $(x_1, x_2, x_3) = (x, y, z)$ and $(u_1, u_2, u_3) = (u, v, w)$.

Our discussion will focus on results obtained by the time-evolving 3DBL generated from an impulsive spanwise-moving wall in a fully developed turbulent channel flow. In the interest of demonstrating the generality of the underlying physics, we will also discuss statistical results from numerical experiments on the Ekman layer, a statistically stationary 3DBL.

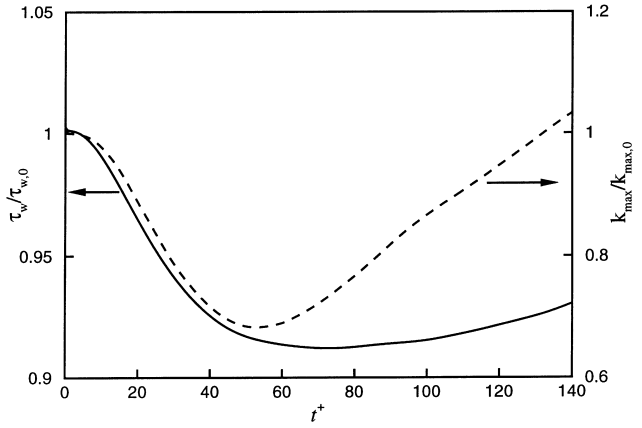

Fig. 1. History of streamwise wall shear and maximum TKE, normalized by value at initial condition, in channel with spanwise moving wall: —— τ_w: ---- k_{max}.

3. Results

The initial fields, at $Re_\tau = 180$, are similar to that of Kim et al. (1987), except that a wider domain with greater streamwise grid resolution is used to accommodate the realignment of the mean flow caused by the moving wall. The results of simulations started from five independent initial fields are averaged into the statistics shown here, three of which have the domain size $4\pi \times 2 \times 8\pi/3$ with $256 \times 129 \times 256$ grid points in the streamwise, wall-normal, and spanwise directions, respectively, and two of which have the domain size $8\pi \times 2 \times 16\pi/3$ with $512 \times 129 \times 512$ grid points. Here, the domain size is normalized by the channel half-height.

Starting from a statistically steady 2D state, the wall is set in motion in the spanwise direction at time $t^+ = 0.0$ with velocity $W_s^+ = -8.5$, generating a spanwise mean shear with positive streamwise vorticity which diffuses from the wall into the flowfield (we use a '+' superscript throughout to indicate scaling with respect to wall units of the *initial* unperturbed flow). Reynolds stress, TKE, and the stress-energy ratio initially decrease, then recover (see Coleman et al., 1996). A corresponding reduction in streamwise wall shear is observed with a similar time scale (Fig. 1). For the sake of discussion, we refer to the time interval when the TKE and streamwise wall shear are decreasing ($t^+ < 60$) as the *reduction* period, with *early reduction* indicating the period when the rate of decrease is accelerating ($t^+ < 20$), and *late reduction* when the decrease is slowing down ($20 < t^+ < 60$). The period during which the drag and peak TKE increase with time from their minima ($t^+ > 60$) is denoted as the *recovery* period.

As we are mainly interested in the mechanisms that reduce turbulence intensity and drag, the present analysis focuses on changes in the flowfield during the reduction period. Throughout this period, the Reynolds stress and mean shear are not aligned, as illustrated in Fig. 2, which shows the development of the lag angle $\lambda = \gamma_s - \gamma_\tau$, where γ_s and γ_τ respectively represent the angles of the mean velocity gradient and turbulent shear stresses in the x–z plane reference frame

$$\gamma_s \equiv \arctan\left(\frac{\partial W/\partial y}{\partial U/\partial y}\right), \quad \gamma_\tau \equiv \arctan\left(\frac{\overline{v'w'}}{\overline{u'v'}}\right).$$

The lag angle decreases in time as the turbulence adjusts to the mean shear. During recovery, the wall-normal variation in the shear angles diminishes and turbulence-mean lag becomes

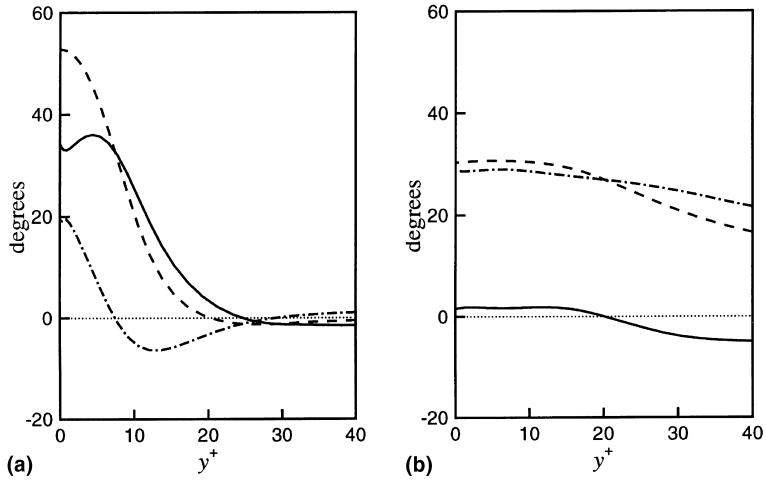

Fig. 2. Shear angles in channel with spanwise moving wall: ---- γ_s, mean shear angle; $- \cdot - \cdot -$ γ_τ, turbulent shear angle; —— λ, lag angle: (a) $t^+ = 13.5$; (b) $t^+ = 135$.

negligible; the flow in the near-wall region therefore becomes *collateral* – i.e., effectively 2D (Fig. 2(b)).

3.1. PDF analysis

Previous research indicated that 3DBLs exhibit asymmetries between the flow induced by vortices having the same and opposite signs of vorticity as the spanwise shear layer (henceforth referred to as *positive* and *negative* vortices, respectively). Assertions have also been made that the sweeps and ejections from near-wall vortices are affected in different ways by the three-dimensionality. We seek to verify these findings by examining the PDFs of the velocity field in the 3D channel flow.

Fig. 3 shows a weighted joint PDF of u' and v' in the 3D channel at $y^+ = 10$, a location where sweeps and ejections are initially similar in strength. The distribution is weighted by $u'v'$, which reveals how each velocity component contributes to the $-\overline{u'v'}$ shear stress. The most important changes to the total Reynolds shear stress early in the flow history are experienced by the streamwise component $-\overline{u'v'}$, since the spanwise fluctuating velocity is slow to respond to the mean spanwise shear. This is demonstrated in Fig. 3(a) and (b), where the u' and v' distributions in the channel coordinates (those aligned with the initial 2D flow) are essentially the same as those that have been aligned with the Reynolds-stress angle γ_τ, implying that the spanwise contribution is insignificant at these times. Later, as the turbulence adjusts to the spanwise perturbation, the spanwise component becomes more significant, which is manifest in the difference between the distributions in the channel frame of reference and that aligned with γ_τ (Fig. 3(c)). These figures show that ejections (events that produce Reynolds shear stress in the second quadrant, or Q2) are affected most significantly by reductions in strong negative u', while sweeps (fourth-quadrant, or Q4, events) are affected by reductions in both u' and v'. Sendstad and Moin (1992) studied a similar time-developing 3D channel flow in which the spanwise shear was created by an impulsive constant pressure gradient. In their DNS study, the effective wall velocity increases linearly from zero, rather than being a step function as in the present case. Nevertheless, much of the behavior of the two flows is similar. They attributed the changes in the fluctuating velocity distribution to modification by the spanwise shear of the trajectories of fluid about streamwise vortices.

To determine the dependence of $-\overline{u'v'}$ on the sign of the streamwise vortex, we condition the weighted joint PDF of u' and v' above with the sign of streamwise vorticity. Fig. 4 reveals that ejections associated with negative ω_x' are reduced to a much greater extent than the sweeps, while the sweeps associated with positive ω_x' are reduced to a much greater degree than ejections. This is consistent with the findings of Sendstad and Moin (1992) and those of Littel and Eaton's rotating disk study (1994), suggesting that the mechanisms affecting the turbulence are the same in both time-evolving and stationary 3DBLs.

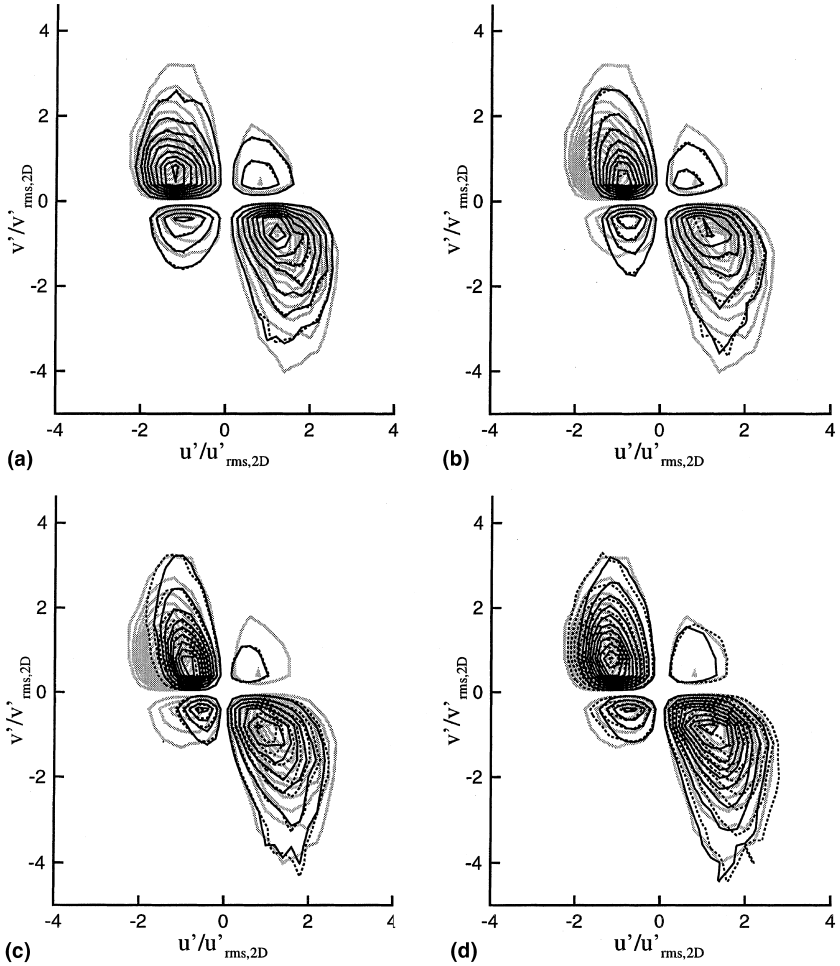

Fig. 3. Weighted joint PDF of u' and v' in channel with spanwise moving wall at $y^+ = 10$: —— 3D distribution; ····· 3D, aligned with Reynolds-stress angle γ_τ; shaded lines denote initial-condition contours: (a) $t^+ = 13.5$; (b) $t^+ = 27$; (c) $t^+ = 54$; (d) $t^+ = 135$.

The joint PDF of streamwise and spanwise vorticity also produces some revealing results. Fig. 5 shows the distribution of vorticity at $y^+ = 10$ at various times for the 3D flow. Unlike the Reynolds shear stress, for which the contour shapes are similar regardless of the frame of reference, the major axis of the vorticity distribution rotates as the flow develops.

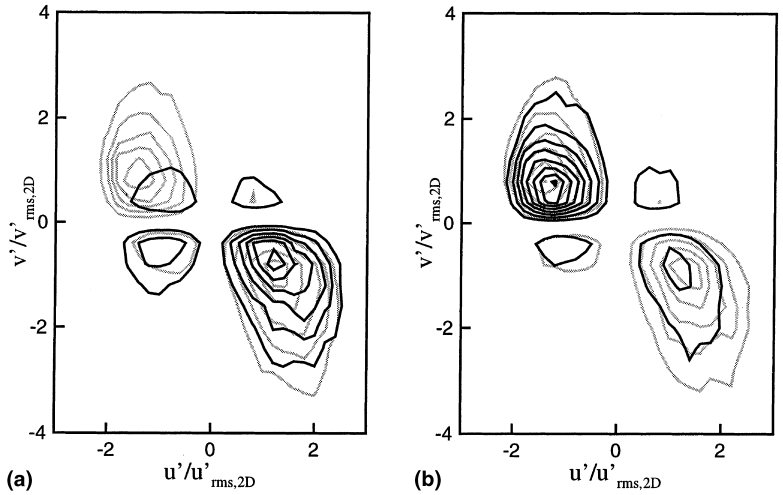

Fig. 4. Weighted joint PDF of u' and v' in channel with spanwise moving wall at $y^+ = 10$ and $t^+ = 13.5$, conditioned on ω_x'; shaded lines denote initial-condition contours: (a) $\omega_x' < 0$; (b) $\omega_x' > 0$.

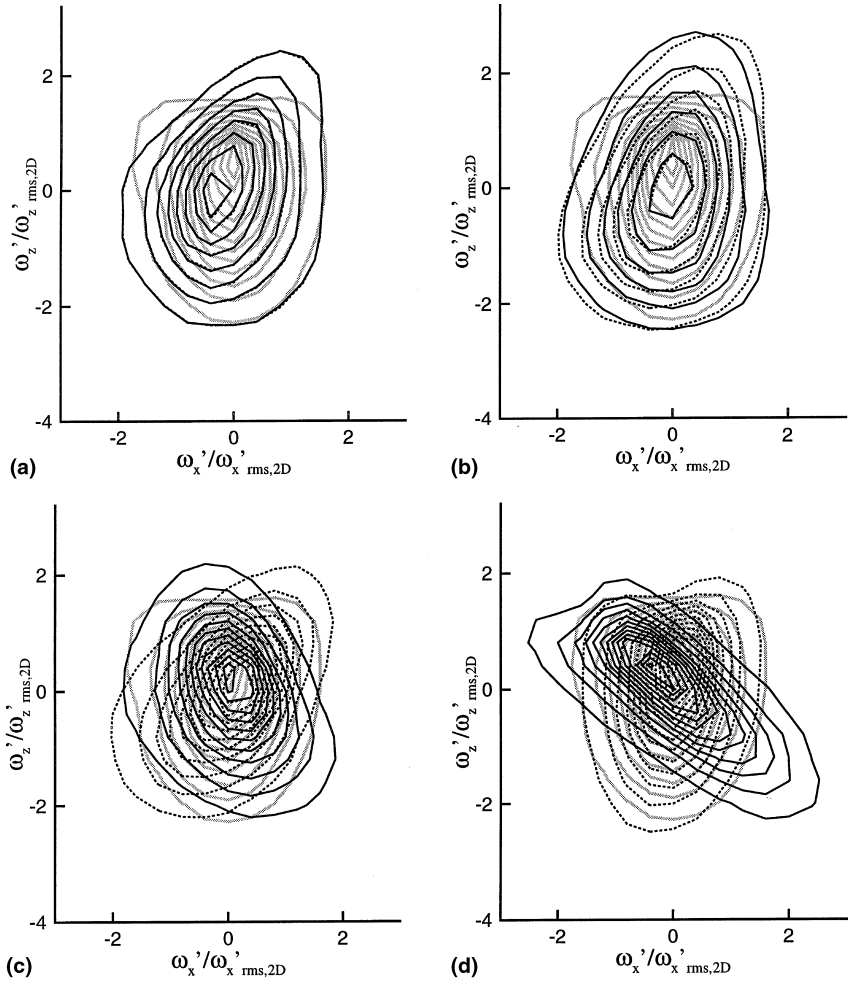

Fig. 5. Joint PDF of ω_x' and ω_z' in channel with spanwise moving wall at $y^+ = 10$: —— 3D distribution, ····· 3D distribution aligned with turbulence intensity angle γ_I; shaded lines denote initial 2D value: (a) $t^+ = 13.5$; (b) $t^+ = 27$; (c) $t^+ = 54$; (d) $t^+ = 135$.

Experience indicates that this rotation is well defined by the *turbulence intensity angle*, γ_I, namely, the orientation of the principal axis of the planar turbulence shear stresses in the x–z plane. This angle is defined as

$$\gamma_I = \frac{1}{2}\arctan\left(\frac{2\overline{u'w'}}{\overline{u'^2} - \overline{w'^2}}\right).$$

In Fig. 5, the dotted lines denote the vorticity distribution in the frame of reference aligned with γ_I. Since the γ_I reference frame accounts for the bulk turning of the vorticity field caused by the moving wall, changes in the shapes of the dotted-curve distribution can be interpreted as evidence of structural modifications of the turbulence.

With the introduction of three-dimensionality, the vorticity magnitude at $y^+ = 10$ increases until $t^+ = 27$, after which it slowly decreases (Coleman et al., 1996). An interesting asymmetry appears in the ω_z' distribution, where positive ω_z' associated with positive ω_x' is increased, while positive ω_z' associated with negative ω_x' is decreased. Note that ω_x' itself does not exhibit appreciable asymmetry. The lack of asymmetry is shown in Fig. 6, where the PDF of ω_x' in the frame of reference aligned with γ_I remains generally symmetric throughout the flow history. This suggests that the vortical structures, which initially are essentially streamwise at this wall-normal location, are not strongly asymmetric in the 3D flow; rather the shear layers or streaks generated by the vortices are affected differently depending on the sign of the vortex. The asymmetry in the spanwise vorticity decreases as the flow recovers.

The contours of u' in the y–z plane shown in Fig. 7 provide a clue to the source of increased spanwise vorticity near the wall. As the wall moves in the spanwise direction, it carries along the fluid next to it, straining the near-wall streaks and causing them to become layered in the wall-normal direction. The resulting velocity gradients, most pronounced at the interface between positive and negative u', represent an increase in spanwise vorticity, ω_z'. It is this layering that increases dissipation during the reduction period, signified by the enstrophy increase observed by Coleman et al. (1996), which contributes to the turbulence kinetic energy reduction. Note that the layering decreases as the turbulence recovers toward a new 2D state.

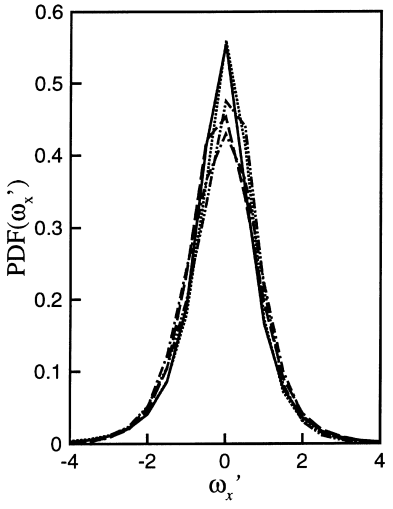

Fig. 6. PDF of streamwise vorticity at $y^+ = 10$ in channel with spanwise moving wall, reference frame aligned with turbulence intensity angle γ_I: —— $t^+ = 0$, ---- $t^+ = 13.5$, – · – · – $t^+ = 27$, – · · – $t^+ = 54$, ····· $t^+ = 135$.

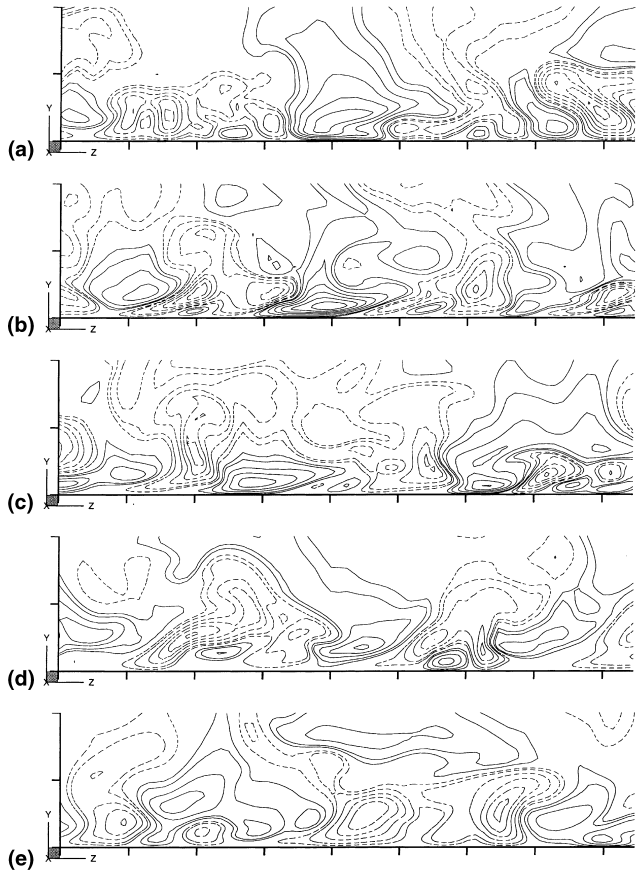

Fig. 7. Contours of u' in y–z plane of channel with a spanwise-moving wall: —— $u' > 0$, ---- $u' < 0$; tickmarks on z-axis represent 50 wall units: (a) initial 2D flow; (b) $t^+ = 13.5$; (c) $t^+ = 27$; (d) $t^+ = 54$; (e) $t^+ = 135$.

We offer an explanation for the ω_z' asymmetry using the schematic diagram in Fig. 8. In a 2DBL, a near-wall streamwise vortex generates a high-speed streak by sweeping high-speed fluid toward the wall and a low-speed streak by ejecting low-speed fluid away from the wall. In the y–z cross-section shown, a positive vortex (one having $\omega_x' > 0$ at its core) has the high-speed streak on the right and the low-speed streak on the left, and vice versa for a negative vortex. In the 3D flow generated by a spanwise-moving wall, the lower part of the streaks move in the spanwise direction, so that the streaks become layered as in Fig. 7. For the positive vortex, the high-speed streak is pulled under the low-speed streak, forming a vertical interface having *positive* ω_z', and lessening the probability of an interface with *negative* ω_z'. Thus, positive ω_z' associated with positive ω_x' is increased, while negative ω_z' associated with positive ω_x' is decreased. A similar effect occurs with the negative vortex, strengthening negative ω_z' associated with negative ω_x', etc. However, since high- and low-speed streaks have different distributions near the wall (high-speed streaks are stronger near the wall, and have wider spanwise extents due to the 'splatting' effect) the near-wall layering associated with the negative vortex is likely to generate a different, perhaps weaker, vertical interface. Thus, the increases in vorticity that occur in the first and third quadrants of the vorticity PDF (in Fig. 5) are not identical. This mechanism is similar to that observed by Dhanak and Si (1999) in their 2D model of a near-wall vortex in the presence of wall oscillations, wherein the oscillations promote the mixing of high- and low-speed streaks.

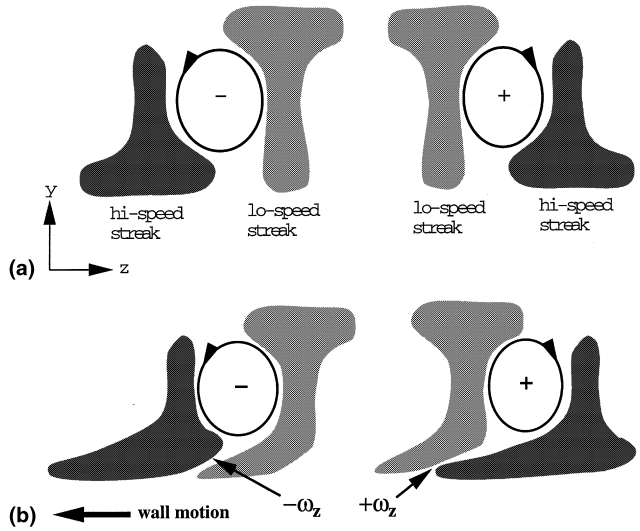

Fig. 8. Schematic of redistribution of vorticity due to streak deformation due to a spanwise-moving wall: (a) initial 2D flow; (b) 3D flow.

3.2. Conditional-averaged quadrant analysis

To isolate the important near-wall structures we examine events that are characteristic of vortical motions. Kang et al. (1998) investigated the velocity fields about strong sweeps and ejections in their rotating disk experiment by averaging about locations containing high Reynolds shear stress, then performing a quadrant analysis on the conditional-averaged quantities. Here we apply the same procedure to the 3D channel flow.

Fig. 9 illustrates the distribution of the Reynolds shear stress about strong sweeps and ejections at $y^+ = 10$ in the 3D channel, *strong* indicating events for which $-u'v' > 2u'_{\mathrm{rms}}v'_{\mathrm{rms}}$, with *sweeps* having $v' < 0$ and *ejections* having $v' > 0$. Here, the frame of reference is aligned with the Reynolds stress angle γ_τ. The center peak in each plot, depicting a strong sweep or ejection, is flanked by two secondary peaks generated by the opposite event. Because near-wall Reynolds shear stress is for the most part associated with near-wall vortical motion, Kang et al. (1998) postulated that these peaks represent the signature of a pair of streamwise vortices that generate the strong Reynolds-stress-producing event. The center peak in each plot contains the combined effect of both vortices, while the secondary peaks contain the effect of an *individual* vortex. Therefore, asymmetries in the Reynolds shear stress production by the vortices can be discerned by comparing the secondary peaks. In Fig. 9(a) the left secondary peak represents the sweep of a *negative* vortex (counter-clockwise with respect to Fig. 9) while the right secondary peak represents the sweep of a *positive* one. Both are dominated by Q4 events. Conversely, in Fig. 9(b) the vortices are positive on the left and negative on the right, and the secondary peaks, dominated by Q2 events, represent ejections from the vortices. Note that at $y^+ = 10$ the Q4 events are more pronounced than the Q2 events in both 2D and 3D flows (the Q4 peaks are more prominent than the Q2 peaks these figures). As z^+ increases, the correlations between structures decrease, and the value of the total conditional average approaches unity, i.e., the average becomes $\overline{u'v'}$ (not conditional). The components from all the quadrants then sum to unity.

In contrast to the roughly symmetric secondary peaks in the initial 2D field (shown as shaded lines), the 3D flow contains significant asymmetries in z of both Q2 and Q4 events at $t^+ = 13.5$, resulting in an asymmetric total stress. Specifically, positive vortices generate both stronger sweeps and ejections, or at least are more effective at generating Reynolds shear stress, than negative vortices. In addition, relative to the plane-averaged $\overline{u'v'}$ at this time, which is decreasing from the 2D level (Fig. 3), strong Q2 and Q4 events are actually stronger than those in the 2D flow, with the strongest events being associated with positive vortices. This suggests that, though there are fewer Reynolds-stress-producing events to contribute to the overall $-\overline{u'v'}$, a greater percentage of the events that do occur generate strong Reynolds shear stress. The positive mean spanwise shear apparently reinforces the effectiveness of positive vortices in generating strong Reynolds shear stress, as previously observed by Anderson and Eaton (1989). Visualization of the 3D flow (discussed below) suggests that this asymmetry in Reynolds shear stress generation is a consequence of the deformation of vortical structures.

Although some asymmetry in Q1 and Q3 events are discernible in Fig. 9, the asymmetry in the total Reynolds shear stress is dominated by the behavior of Q2 and Q4 events. This is in contrast to the findings of Kang et al. (1998), who found that the asymmetries in the total Reynolds-stress are only due to Q1 and Q3 events. However, their measurements were

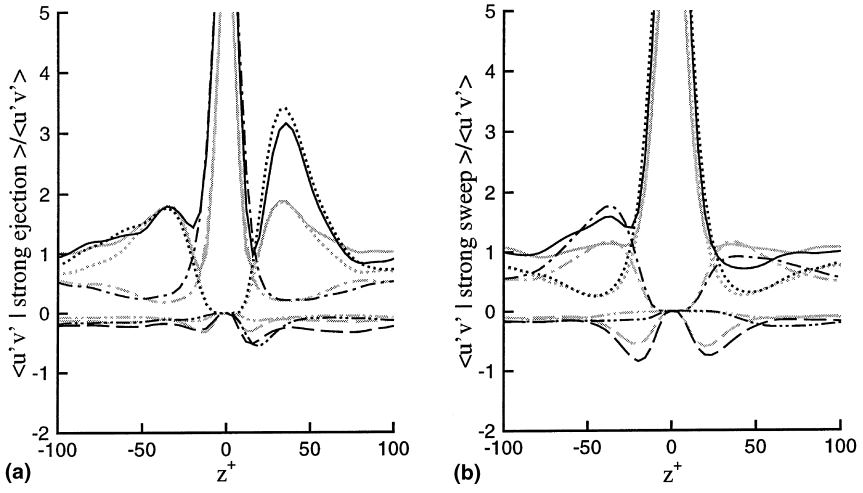

Fig. 9. Conditional average of $u'v'$ at $y^+ = 10$ in channel with spanwise moving wall, $t^+ = 13.5$: —— total $\langle u'v' \rangle$; ---- Q1; – · – · – Q2; – · · – Q3; · · · · · · · Q4; shaded lines denote initial-condition contours: (a) strong ejection; (b) strong sweep.

taken at $y^+ \approx 90$, much further away from the wall than in the results plotted in Fig. 9. The 3DBL in their rotating disk experiment is also statistically stationary, rather than time-evolving as in the present study. For more direct comparisons we perform the same quadrant analysis on the Ekman layer of Coleman (1999), also a statistically stationary 3DBL with a similar spanwise mean velocity profile (Reynolds number for this flow is $Re \equiv U_\infty D/\nu = 1000$, where U_∞ is the magnitude of the freestream velocity, and $D^2 = \nu/\Omega$, with Ω being the rate of rotation about the wall-normal axis). Fig. 10 reveals that at $y^+ = 10$ the Reynolds shear stress possesses the asymmetries observed in the channel with a spanwise moving wall, while Fig. 11 shows only a slight asymmetry at $y^+ = 89$, which is still characterized by differences in the Q2 and Q4 peaks. Thus, the asymmetries observed in the total Reynolds shear stress (Figs. 9–11) come from Reynolds-stress-producing quadrants. Moreover, at the larger wall-normal distance, Reynolds shear stress is not typically associated with quasi-streamwise vortices, which exhibit the asymmetric behavior we observe, but with, for instance, the heads of hairpin vortices, which may respond differently to mean three-dimensionality.

3.3. Visualization

Finally, we visualize the vortical structures in the channel flow using isosurfaces of λ_2. Fig. 12 shows an example for the 2D case. The vortices are oriented roughly in the streamwise direction, and arranged in an overlapping manner. Jeong et al. (1997), who performed a conditional average on the λ_2 distribution in a channel flow, described the alignment of the near-wall vortices as the alternating positive–negative pattern presented schematically in Fig. 16(a). Such clustering of vortical structures allows them to reinforce each other's induced flowfields, giving rise to streaks whose lengths are many times longer than the vortices themselves. Fig. 13, in which ω_y' contours represent the streak boundaries at $y^+ = 5$, clearly demonstrates this characteristic. Jeong et al. (1997) also showed that the average near-wall vortex is not aligned with the x-axis, but is slightly rotated in the x–z plane as shown in Fig. 16(a), and inclined in the wall-normal direction, so that the downstream head of the vortex is further away from the wall than the tail.

Fig. 14 displays the effect of the spanwise shear upon the vortical structures at $t^+ = 13.5$. Although the vortical struc-

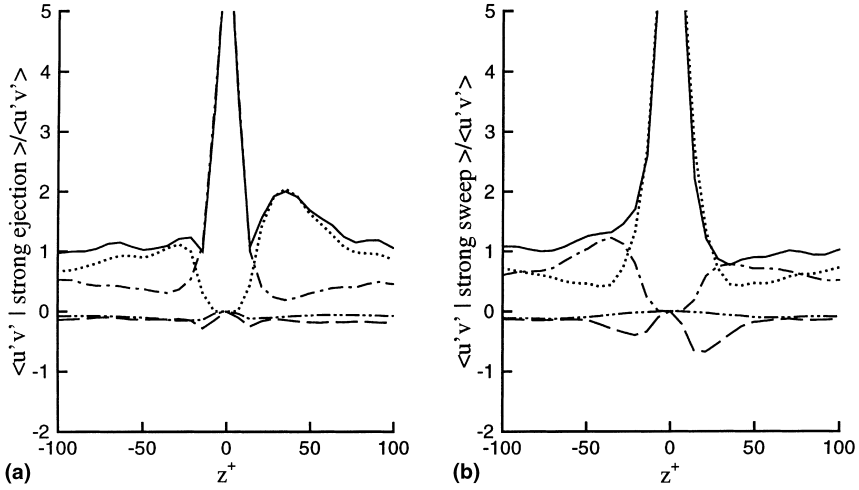

Fig. 10. Conditional average of $u'v'$ in Ekman layer at $y^+ = 10$; symbols same as in Fig. 9: (a) strong ejection; (b) strong sweep.

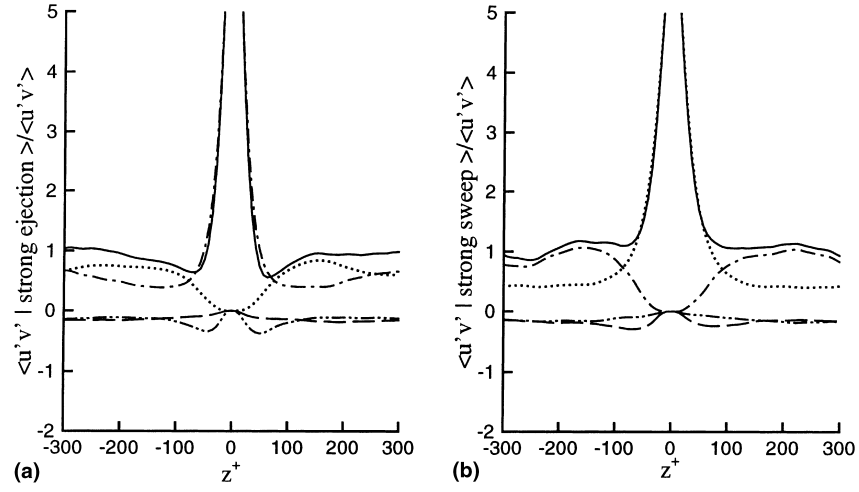

Fig. 11. Conditional average of $u'v'$ in Ekman layer at $y^+ = 89$; symbols same as in Fig. 9: (a) strong ejection; (b) strong sweep.

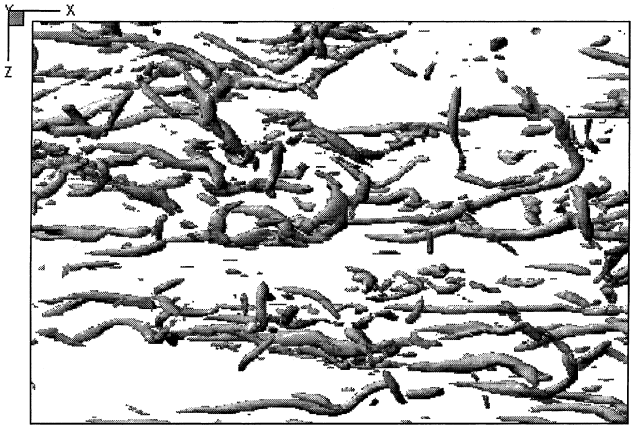

Fig. 12. Vortices in initial 2D channel ($t^+ = 0$): isosurfaces of $\lambda_2 = -0.012$, scaled with wall units.

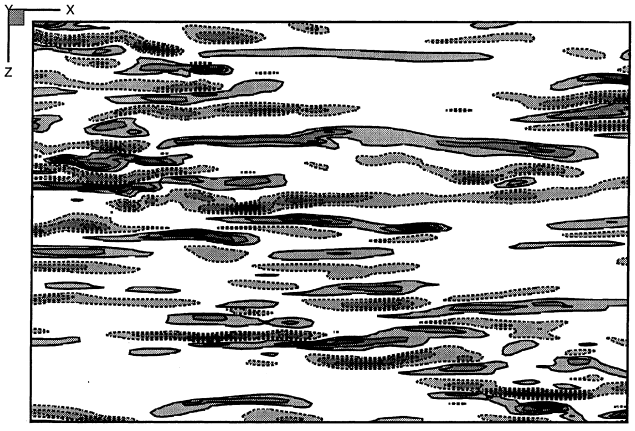

Fig. 13. Wall-normal vorticity in 2D channel ($t^+ = 0$) at $y^+ = 5$: —— $\omega'_y > (\omega'_{y,0})_{\mathrm{rms}}$; ····· $\omega'_y < -(\omega'_{y,0})_{\mathrm{rms}}$, where $(\omega'_{y,0})_{\mathrm{rms}} \equiv (\overline{\omega'_y \omega'_y})^{1/2}$ in initial 2D flow; contour levels incremented by $(\omega'_{y,0})_{\mathrm{rms}}$.

tures are not diminished to an appreciable degree at this time, the tails of the vortices, which are closer to the wall, move with the wall in the spanwise direction, while the heads retain their 2D orientation. This results in a change in the shapes of the vortices. Notice that many of the vortices in Fig. 14 appear to have more curvature than those in Fig. 12, and that the streaks shown in Fig. 15 appear to be breaking up into shorter structures that exhibit some degree of realignment in the new mean shear direction.

Based on the statistical and visualization results, we offer Fig. 16 as a model of the changes in vortical structures in a 3DBL. In contrast to the relatively symmetric structures shown in Fig. 16(a), positive vortices are now 'J-shaped', and negative vortices 'S-shaped'. Because the induced velocity on the concave side of a vortex line is greater than on the convex side, positive vortices create weaker sweeps than ejections, and negative vortices have weaker ejections than sweeps, resulting in the asymmetries observed in the velocity PDFs. Moreover, because the single-curvature of a positive vortex tends to focus its ejections more than the double-curvature of a negative vortex reinforces its sweeps, the Reynolds shear stress generated by positive vortices is stronger than that of negative vortices, which is manifest in the asymmetric distribution in the conditional-averaged quadrant analysis (Fig. 9). Another effect of the spanwise shear is to rotate the vortices away from their cooperative, overlapping alignment, resulting in the break-up of the nearwall streaks, as seen in Fig. 15.

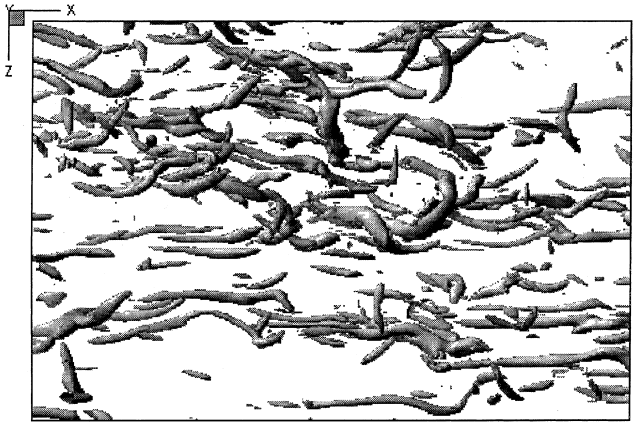

Fig. 14. Vortices in channel with spanwise moving wall at $t^+ = 13.5$: symbols same as in Fig. 12. Wall motion is in negative z-direction.

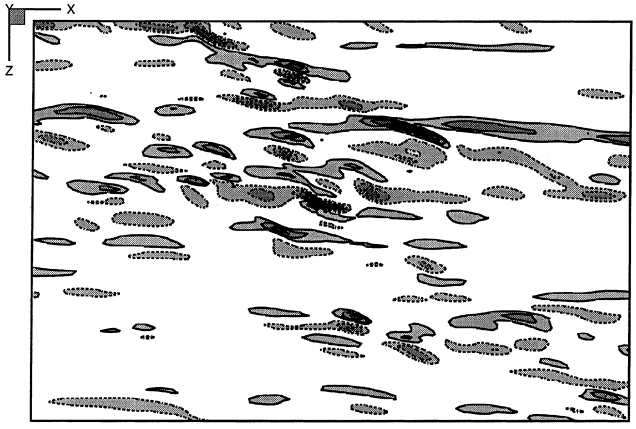

Fig. 15. Wall-normal vorticity in channel with spanwise-moving wall at $y^+ = 5$ and $t^+ = 13.5$: symbols same as in Fig. 13. Wall motion is in negative z-direction.

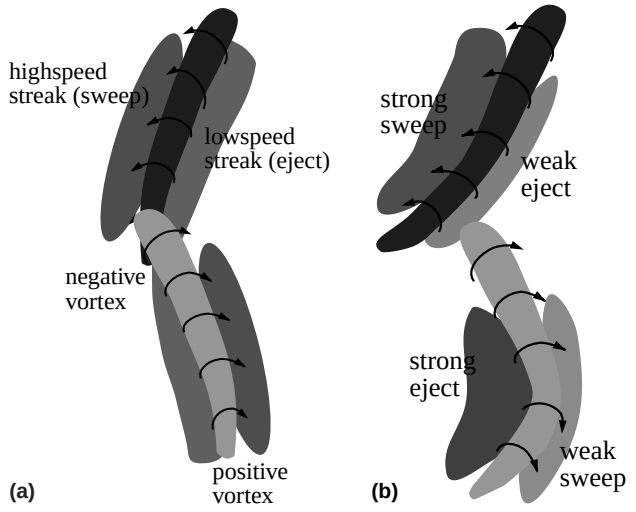

Fig. 16. Schematic of near-wall turbulence structures in (a) 2DBL and (b) 3DBL.

In the case of the 3D channel, the TKE, Reynolds shear stress and drag eventually recover as the near-wall structures realign themselves in the direction of the mean shear. Symmetry is restored in the Reynolds stress production, and the stress–strain lag angle returns to zero. In 3DBLs where mean three-dimensionality is maintained in a stationary state (such as the Ekman layer or the flow over a rotating disk), the lag angle remains finite and the efficiency of the flow in generating turbulence is generally reduced, as implied by the decrease in the stress/energy ratio often observed in these flows.

4. Summary and conclusions

DNS of a channel with a spanwise-moving wall has been used to examine the effects of mean three-dimensionality on near-wall turbulence structures that lead to reduced turbulence intensity and drag. PDFs and conditional-averaged quadrant analysis reveal that the three-dimensionality affects positive and negative vortices in different ways, thus destroying the spanwise symmetry of the turbulence structures. Visualizations show that the asymmetries arise due to temporary changes in the shapes of the vortical structures, and the reduction in streak size and strength are due to the alignment of the vortices being altered. The mean spanwise shear also increases the TKE dissipation by causing wall-normal layering of the streaks. These effects reduce the ability of the mean velocity gradient to sustain the turbulence, resulting in the reductions in TKE and drag characteristic of 3DBLs.

Acknowledgements

This work is supported by the Office of Naval Research (Grant No. N-00014-94-1-0016). Computing resources are provided by NASA-Ames Research Center and the National Partnership for Advanced Computational Infrastructure at the San Diego Supercomputer Center.

References

Anderson, S.C., Eaton, J.K., 1989. Reynolds stress development in a pressure driven three-dimensional turbulent boundary layer. Journal of Fluid Mechanics 202, 263–294.

Coleman, G.N., 1999. Similarity statistics from a direct numerical simulation of the neutrally stratified planetary boundary layer. Journal of Atmospheric Sciences 56, 891–900.

Coleman, G.N., Kim, J., Le, A.-T., 1996. A numerical study of three-dimensional wall-bounded flows. International Journal of Heat and Fluid Flow 17, 333–342.

Coleman, G.N., Kim, J., Spalart, P.R., 1997. Direct numerical simulation of decelerated wall-bounded shear flows. In: Proceedings of the 11th Turbulent Shear Flows Conference, Grenoble, France.

Dhanak, M.R., Si, C., 1999. On reduction of turbulent wall friction through spanwise wall oscillations. Journal of Fluid Mechanics 383, 175–195.

Jeong, J., Hussain, F., 1995. On the identification of a vortex. Journal of Fluid Mechanics 285, 69–94.

Jeong, J., Hussain, F., Schoppa, W., Kim, J., 1997. Coherent structures near the wall in a turbulent channel flow. Journal of Fluid Mechanics 332, 185–214.

Johnston, J.P., Flack, K.A., 1996. Review – advances in three-dimensional turbulent boundary layers with emphasis on the wall-layer regions. Journal of Fluids Engineering 118, 219–232.

Kang, S.K., Choi, H., Yoo, J.Y., 1998. On the modification of the near-wall coherent structure in a three-dimensional turbulent boundary layer on a free rotating disk. Physics of Fluids 10, 2315–2322.

Kim, J., Moin, P., Moser, R., 1987. Turbulence statistics in fully developed channel flow at low Reynolds number. Journal of Fluid Mechanics 177, 133–166.

Littel, H.S., Eaton, J.K., 1994. Turbulence characteristics of the boundary layer on a rotating disk. Journal of Fluid Mechanics 266, 175–207.

Sendstad, O., Moin, P., 1992. The near wall mechanics of 3D turbulent boundary layers. Report No. TF-57, Thermosciences Div., Dept. Mech. Engr., Stanford University, Stanford, CA.

Shizawa, T., Eaton, J.K, 1990. Interaction of an embedded longitudinal vortex with an attached, 3D turbulent boundary layer. Report No. TF-56, Thermosciences Div., Dept. Mech. Engr., Stanford University, Stanford, CA.

Tomkins, C.D., Adrian, R.J., Balachandar, S., 1998. The structure of vortex packets in wall turbulence. In: Proceedings of the 29th Fluid Dynamics Conference, Albuquerque, NM.